ELSEVIER

Journal of Crystal Growth 148 (1995) 305–323

JOURNAL OF CRYSTAL GROWTH

Steady-state solutions for an array of strongly-interacting needle crystals in the limit of small undercooling

Brian J. Spencer, Herbert E. Huppert

Institute of Theoretical Geophysics, Department of Applied Mathematics and Theoretical Physics, University of Cambridge, Silver Street, Cambridge CB3 9EW, UK

Received 25 August 1994; manuscript received in final form 28 November 1994

Abstract

We consider the free-boundary problem for the steady-state solidification of a pure undercooled liquid in the form of an array of three-dimensional needle crystals. We neglect surface energy, consider the limit of small undercooling, and solve for the crystal shape analytically using slender body theory. The solutions have two degrees of freedom which determine the growth velocity as a function of the tip radius and the array spacing. For large array spacings we recover the Ivantsov similarity solution for an isolated dendrite, while for small array spacings the strong interactions between neighboring dendrites cause the Peclet number of the dendrite tip to be determined by an array-modified undercooling. Our leading-order results are valid for any space-filling array pattern and apply to solidification in channels of various shapes. The results can also be adapted to describe solidification of a two-component supersaturated solution at uniform temperature by making the one-sided approximation.

1. Introduction

For a number of decades the well-known Ivantsov dendrite [1] has been a cornerstone in the theory of dendritic growth. The Ivantsov similarity solution describes the steady-state growth of an isolated dendrite from an undercooled one-component melt in the absence of surface energy. The dendrite shape is that of a three-dimensional paraboloid of revolution which grows at constant speed V and tip radius ρ. The similarity solution determines the product ρV in terms of the undercooling but does not provide for the selection of a unique velocity.

Experimental studies of the growth of free dendrites [2] reveal two important facts regarding the importance of the Ivantsov solution. Firstly, for a given undercooling there is a unique growth velocity for the free dendrite. Secondly, in situations where convection in the liquid is negligible, the dynamics of the dendrite tip are accurately described by the Ivantsov solution: the predictions of ρV in terms of the undercooling are in excellent agreement with the experimental data [2]. Thus, even though there is no provision for velocity selection in the Ivantsov solution, it is fundamental to the theoretical description of free dendrites.

The prediction of the unique growth velocity for the free dendrite is an important problem in

0022-0248/95/$09.50
SSDI 0022-0248(94)00965-1

crystal growth that has not yet been satisfactorily resolved. While it is generally agreed that surface energy provides the additional length scale necessary for the selection of a unique growth velocity and tip radius, the actual mechanism by which selection occurs is not clear. Among the more recent selection theories are marginal stability theory [3], microsolvability theory [4,5], and interfacial wave theory [6]. While the details of selection in these theories are different, a common feature to all is the Ivantsov dendrite. This is because the presence of surface energy, although responsible for the theoretical selection of a unique tip radius, results in only a small correction to the shape of the Ivantsov solution in the tip region. For this reason, whatever the details of the selection mechanism turn out to be, the Ivantsov solution will be fundamental to the description of free-dendrite growth.

An important long range goal in studying solidification, however, is to build a description of an array of dendrites, as typically occurs during solidification processes. The spacing between dendrites in these arrays is an important characteristic of the solidification morphology, and plays a large role in determining the mechanical properties of the solidified product [7]. The dendrite spacing itself is determined as part of the growth process by a competitive interaction between the dendrites in the array. A useful theory of array growth, then, must be able to describe these interactions. Clearly the isolated dendrite represents the case of infinitely large array spacing. When the spacing is finite the dendrites in the array must influence one another in some way. The purpose of this paper is to determine how the Ivantsov dendrite is modified when it is part of an array. These modified solutions are a basis for the description of the growth of arrays of dendrites in the same way as the Ivantsov dendrite is the basis for the description of the growth of free dendrites.

While there has not been a theoretical treatment which describes how the three-dimensional Ivantsov dendrite is modified when part of an array, there have been two theoretical papers which describe how the Ivantsov dendrite is modified when growing in an insulated channel [8,10]. Solidification in a channel is closely related to array growth because the symmetry conditions of a spatially-periodic array correspond to the no-flux boundary conditions of the insulated channel. Pelce and Pumir [8] have studied the solidification of a two-dimensional dendrite in a two-dimensional channel. By considering the limit where the channel width is much smaller than the diffusion length they found that the steady-state shape of the needle crystal could be described using the theory developed for Saffman–Taylor fingers in Hele–Shaw flow [9]. The finger-like shapes for the needle crystal were determined analytically and had two degrees of freedom – one is the unknown velocity as in the Ivantsov solution for the free dendrite and the other is the channel width. Hunt [10] has studied dendritic growth in an axisymmetric cylinder as an approximation to a hexagonal channel. The dendrite is thus three-dimensional but axisymmetric. The governing equations were solved numerically to determine the steady-state shape as a function of the cylinder diameter. In the absence of surface energy the finger-like solutions have two degrees of freedom which correspond to the cylinder size (dendrite spacing) and the growth speed. As the cylinder size approaches infinity the Ivantsov solution is recovered. Although the results do not correspond to an array in a strict sense, the results can be thought of as approximating a hexagonal array with the degree of approximation given by how well a circle approximates a hexagon.

Warren and Langer [11,12] consider a fully three-dimensional array of dendrites during directional solidification of a binary alloy. They look for steady-state solutions in the form of a repeating-square array of identical dendrites. They assume that the dendrite shape can be described by a paraboloid of revolution and further assume that the dendrite interactions are sufficiently weak that the tip radius of each dendrite is given by the solvability theory for the free dendrite. They then determine numerically a one-parameter family of steady-state solutions that depends on the dendrite spacing. Their steady-state solutions are compatible with experimentally observed dendritic arrays [13], provided that the dendrite spacing λ is not too small

relative to the diffusion length l. When $\lambda < l$ they suggest that the interactions between the dendrites lead to deviations from a paraboloidal shape. It is precisely these deviations we seek to describe.

Our approach is similar to that of Warren and Langer [11] in that we look for steady-state solutions in which the solidification front consists of a regular array of identical dendrites. For definiteness we take the array to have the pattern of repeating squares. However, we consider the simpler problem of solidification of a pure material and will neglect surface energy, as is usual for the Ivantsov dendrite. We plan to investigate the solidification of a two-component system in a subsequent paper. The important new ingredient here is our incorporation of strong interactions between the dendrites. While the numerical solutions of Hunt [10] for the axisymmetric dendrite capture the flavor of these dendritic interactions, there is also a need for an analytic description of a fully three-dimensional array. In particular, the numerical calculations for the axisymmetric case run into difficulties when the undercooling is small and the dendrites are slender relative to the radius of the cylindrical channel. This discrepancy in scales, which leads to numerical difficulties, can be exploited by asymptotic means to describe the dendrite shape. Our aim in this paper, then, will be to develop an analytic description for steady-state arrays of slender, strongly interacting dendrites.

We begin with the governing equations for the free-boundary problem that describes the steady-state growth of a regular (square) array of identical dendrites with prescribed spacing λ (see Fig. 1). In the limit of $\lambda \to \infty$ these equations are satisfied by the Ivantsov solution. In general the governing equations cannot be solved analytically, but we are able to make progress by considering the limit of small undercooling. In this limit the dendrites are thin: if a is a characteristic radius of the dendrite, then $a \ll \lambda$. We exploit this disparity in length scales to construct an analytic solution for the array as an asymptotic series in the small undercooling. In these solutions the degree of interaction between the tip of a given dendrite and its neighbors will depend on the size

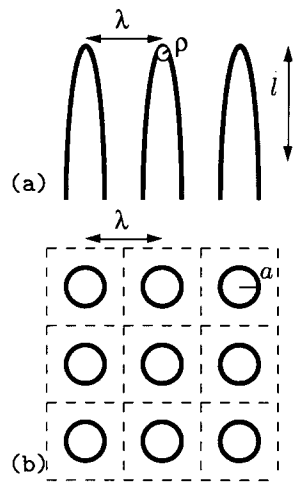

Fig. 1. Schematic of dendrite array: (a) side view, (b) top view. The array length scales are the tip radius ρ, dendrite radius a, spacing λ and diffusion length l. The roots of the dendrites are parallel far behind the tips.

of the spacing λ compared to the diffusion length l (= diffusivity/growth speed). If λ is sufficiently large the tips of the dendrites are not significantly influenced by the array. In contrast, we restrict our attention to those spacings for which the tips of the dendrites *are* influenced significantly by the array. With this in mind, we are able to choose a scaling for λ/l which captures the smooth transition from weakly-interacting tips, where the tip dynamics are described by free-dendrite theory, to strongly-interacting tips, where the tip dynamics are considerably modified by the presence of the array. In these scalings the characteristic lengths are ordered $\rho \ll a \ll \lambda \ll l$. A consequence of these scalings is that the dendrite approaches equilibrium at a distance of $O(l)$ behind the dendrite tips. The dendrites themselves thus appear long and slender. The free-boundary problem for the dendrite shape can then be solved using slender-body theory [14] to obtain an analytic description of the dendrite shape and the associated temperature field. This is done by first solving the governing equations in the near dendrite, inter-dendrite and tip regions (see Fig. 2). Then, by matching the three solutions in the appropriate overlap regions we establish a uniformly valid solution to the free-boundary problem. Our results provide a new analytic solution

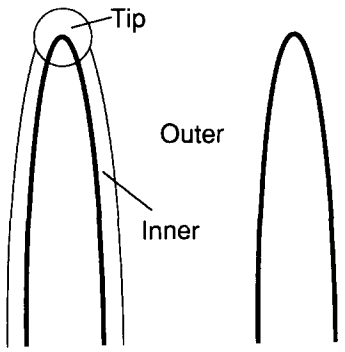

Fig. 2. Schematic of the three regions in which the equations are solved. Inner denotes the near-dendrite region and outer denotes the inter-dendrite region.

for the growth of arrays of interacting needle crystals in three dimensions. The effect of the array is to generate a *modified undercooling* at the dendrite tips which alters ρV from that of the Ivantsov solution.

The rest of the paper is organized as follows. In Section 2 we derive the governing equations that define the free-boundary problem for the steady-state dendritic array. In Section 3 we consider the limit of small undercooling and introduce the scalings appropriate for describing slender, interacting dendrites. We then outline the solution procedure and solve the equations in the inner (near-dendrite); outer (inter-dendrite); and tip regions. Details of matching the solutions appear in the Appendices. Our results are presented in Section 4 and the main conclusions summarized in Section 5.

2. Steady-state dendritic arrays

Our aim is to develop an analytical description of a steady-state solidification front consisting of an array of parallel dendrites growing into an undercooled liquid. We begin with the usual equations describing the solidification of a pure material. The major assumptions behind this description are: (1) the solid–liquid boundary is assumed to be in local thermodynamic equilibrium; (2) the effect of surface energy is negligible; (3) there is no volume change upon solidification; and (4) the material properties are constant and isotropic. Under these assumptions the temperature of the liquid, $T(X, Y, Z, t)$ is governed by the diffusion equation

$$\frac{\partial T}{\partial t} = \kappa \nabla^2 T \quad \text{in the liquid,} \tag{2.1}$$

where κ is the thermal diffusivity. The solid–liquid boundary, denoted by $\mathscr{B}$, is a free boundary whose location is determined as part of the solution. The temperature on $\mathscr{B}$ is given by local equilibrium as

$$T = T_M \quad \text{on } \mathscr{B}, \tag{2.2}$$

where T_M is the melting temperature. In what follows we shall concern ourselves exclusively with solidification of an undercooled melt. In this case the temperature in the solid remains identically at the melting temperature with

$$T = T_M \quad \text{in the solid.} \tag{2.3}$$

Conservation of energy at the solid–liquid boundary gives a balance between the release of latent heat and the diffusion of heat away from the boundary. This balance takes the form

$$LV_n = -\kappa c_p (\boldsymbol{n} \cdot \nabla T) \quad \text{on } \mathscr{B}, \tag{2.4}$$

where L is the latent heat per unit mass, c_p is the heat capacity of the liquid, $\boldsymbol{n}$ is the normal vector to $\mathscr{B}$ pointing into the liquid, and V_n is the velocity of the boundary in the direction of $\boldsymbol{n}$. We take the direction of growth to be $+Z$. Solidification is driven by an undercooled liquid in the far field,

$$T \to T_M - \Delta T \quad \text{as } Z \to \infty \text{ in the liquid.} \tag{2.5}$$

Eqs. (2.1)–(2.5) define the free-boundary problem for solidification of an undercooled melt. The Ivantsov dendrite [1] is a steady-state solution in which $\mathscr{B}$ is a paraboloid of revolution translating along its axis at speed V in the $+Z$ direction. We seek to determine how this steady-state solution is modified when it is part of an array of dendrites. To this end we use a moving coordinate system which translates at constant speed V in the $+Z$ direction. We nondimensionalize lengths on the diffusion length $l = \kappa/V$, and

introduce the dimensionless coordinates in the moving frame as

$$(x, y, z) = \frac{1}{l}(X, Y, Z - Vt). \tag{2.6}$$

We choose our coordinate system such that $z = 0$ corresponds to the tips of the dendrites in the array. At this time it is also convenient to introduce dimensionless (tilded) versions of the characteristic array length scales appearing in Fig. 1,

$$(\tilde{\rho}, \tilde{a}, \tilde{\lambda}) = \frac{1}{l}(\rho, a, \lambda). \tag{2.7}$$

These dimensionless lengths are all Peclet numbers based on different length scales of the morphology. The dimensionless tip radius $\tilde{\rho}$ is often called *the* Peclet number for dendritic growth. We also let $\Theta(x, y, z)$ be the dimensionless steady-state temperature defined by

$$\Theta = \frac{T - (T_M - \Delta T)}{\Delta T}, \tag{2.8}$$

and define the dimensionless undercooling parameter σ (the inverse Stefan number) as

$$\sigma = c_p \Delta T / L. \tag{2.9}$$

The dimensionless steady-state versions of Eqs. (2.1)–(2.5) are then

$$\nabla^2 \Theta + \frac{\partial \Theta}{\partial z} = 0 \quad \text{in the liquid,} \tag{2.10}$$

$$\Theta = 1 \quad \text{on } \mathscr{B}, \tag{2.11}$$

$$\Theta = 1 \quad \text{in the solid,} \tag{2.12}$$

$$n_z + \sigma(\boldsymbol{n} \cdot \nabla \Theta) = 0 \quad \text{on } \mathscr{B}, \tag{2.13}$$

and

$$\Theta \to 0 \quad \text{as } z \to \infty \text{ in the liquid,} \tag{2.14}$$

where n_z is the z component of $\boldsymbol{n}$.

For any steady-state array there must exist a state of equilibrium far behind the dendrite tips in which the solid and liquid are both uniformly at the melting temperature. This means that

$$\Theta \to 1 \quad \text{as } z \to -\infty \text{ in the liquid.} \tag{2.15}$$

A consequence of this equilibrium state is a predetermination of the amount of solid at equilibrium since the originally undercooled liquid can only absorb a finite amount of latent heat before reaching the equilibrium melting temperature. An energy balance between the heat content of the undercooled liquid as $z \to +\infty$ and the heat content of the equilibrium solid/liquid mixture as $z \to -\infty$ prescribes the equilibrium volume fraction of solid ϕ as

$$\phi = \sigma. \tag{2.16}$$

Since $\phi > 1$ is nonphysical and $\phi = 1$ corresponds to plane-front solidification, steady-state array solutions are only possible if $\sigma < 1$.

We now look for specific solutions to the steady-state free boundary problem defined by Eqs. (2.10)–(2.16) in the form of a periodic array of dendrites (see Fig. 1). The solidification front is taken to consist of an array of unit cells which are periodic in x and y and extend from $z = -\infty$ to $z = +\infty$. In the center of each cell is a single dendrite, and all the dendrites are identical. The cell cross-sections could be any shape that produces a repeating pattern, such as squares, rectangles or hexagons. From the cross-sectional area of the cell, A_{cell}, we define the dimensionless dendrite spacing $\tilde{\lambda}$ as

$$\tilde{\lambda}^2 = A_{\text{cell}}. \tag{2.17}$$

For definiteness we shall take the cells to be square in cross section. Each cell is indexed by position, with cells centered at $x = i\tilde{\lambda}$, $y = j\tilde{\lambda}$ with i and j ranging over all the integers. The surface of each dendrite $\mathscr{B}$ is described in cylindrical coordinates (r, z, θ) relative to the center axis of its cell by $r = \tilde{R}(z, \theta)$. From the dendrite shape comes the dimensionless mean radius of curvature at the dendrite tip $\tilde{\rho}$ and the characteristic dimensionless dendrite radius $\tilde{a}$. Formally, we define $\tilde{a}$ by the effective cross-sectional radius of the equilibrium dendrite,

$$\pi \tilde{a}^2 = \lim_{z \to -\infty} \int_0^{2\pi} \int_0^{\tilde{R}(z,\theta)} r \, dr \, d\theta. \tag{2.18}$$

The conservation of energy condition (2.16) then relates the equilibrium radius $\tilde{a}$ to the spacing $\tilde{\lambda}$ as

$$\pi \tilde{a}^2 = \sigma \tilde{\lambda}^2. \tag{2.19}$$

3. The limit of small undercooling

The system (2.10)–(2.16) still represents a difficult free-boundary problem for the shape $\tilde{R}(z, \theta)$. In general the dendrite shape is nonaxisymmetric because a given dendrite feels the nonaxisymmetric temperature field generated by its neighbors. This temperature field varies laterally on the scale of the dendrite spacing $\tilde{\lambda}$. When the dendrite radius $\tilde{a} \ll \tilde{\lambda}$, however, the asymmetry disappears at leading order. In this limit a given dendrite only samples the temperature field generated by the array along a vertical line. To the dendrite, the array modifies the temperature field in a way that varies in the vertical direction only, and to first approximation the dendrite is axisymmetric. This leading order axisymmetry can be guaranteed by considering the small undercooling limit $\sigma \ll 1$ which assures $\tilde{a} \ll \tilde{\lambda}$ by (2.19).

Consider then the limit of small undercooling $\sigma \ll 1$. We determine the scaling for tip radius $\tilde{\rho}$ in terms of σ from the Ivantsov solution at small undercooling. The Ivantsov solution satisfies [1]

$$\sigma = (\tilde{\rho}/2) E_1(\tilde{\rho}/2) \exp(\tilde{\rho}/2), \tag{3.1}$$

where $E_1(x) = \int_x^\infty (e^{-s}/s)\, ds$ is the exponential integral. When $\sigma \ll 1$ it follows from (3.1) that

$$\sigma = O[\tilde{\rho} \ln(1/\tilde{\rho})]. \tag{3.2}$$

While we do not expect that (3.1) will necessarily describe array growth (it is only true if $\tilde{\lambda} = \infty$), we do expect that the scaling (3.2) will be appropriate as long as $\tilde{\lambda}$ is not too small. How small $\tilde{\lambda}$ can be for this scaling to apply will be addressed shortly. Now, however, we introduce scalings for $\tilde{\rho}$ and σ which preserves relationship (3.2). Since this relationship is not easily inverted to find $\tilde{\rho}$ in terms of σ, we introduce a small parameter $\epsilon \ll 1$ to measure the smallness of the undercooling. For convenience we define ϵ from

$$\sigma = \epsilon^2 \ln(1/\epsilon). \tag{3.3}$$

Having defined ϵ in this way the proper scaling for $\tilde{\rho}$ is determined from (3.2) as

$$\tilde{\rho} = \epsilon^2 P, \tag{3.4}$$

where $P = O(1)$ is a scaled Peclet number.

At this point the size of the array spacing $\tilde{\lambda}$ is still not prescribed. The size of $\tilde{\lambda}$ determines the strength of interactions between the dendrite tips. For large $\tilde{\lambda}$ the dendrites interact only very weakly – the temperature field near a given dendrite tip is (to leading order) the same as what it would be for an isolated dendrite. If we choose $\tilde{\lambda} = O(1)$ it turns out that the interactions are also weak and the leading-order dynamics of each dendrite tip are described by the Ivantsov solution. In order to describe "strong interactions" between dendrites it is necessary to consider $\tilde{\lambda} \ll 1$. The transition from weakly-interacting dendrites to strongly-interacting dendrites occurs when the tip of each dendrite feels the rest of the array as an O(1) contribution to the temperature field. The scaling for $\tilde{\lambda}$ that captures this transition can be determined as follows. Consider first an array of dendrites which are well-separated. In this limit, each dendrite behaves as if it were isolated and can be described by the Ivantsov dendrite. As mentioned by Canright and Davis [15] the Ivantsov solution can be generated by a half-line source of heat moving steadily along its length. A straightforward calculation shows that in the moving frame the Ivantsov solution can be recovered by using a stationary half-line source of constant strength q_0, where $q_0 = 4\pi/E_1(\tilde{\rho}/2)$, and where $\tilde{\rho}$ is related to the undercooling by (3.1). For small undercoolings we have $\tilde{\rho} = O(\epsilon^2)$ by (3.4) and thus the heat source is weak with $q_0 = O[1/\ln(1/\epsilon)]$. The magnitude of the temperature field generated by an array of these line sources is given by the product of the source strength and the number of sources per unit area of the array, $q_0/\tilde{\lambda}^2$. Thus, for the O(1) temperature field associated with strongly-interacting dendrites we must choose $\tilde{\lambda} = O([1/\ln(1/\epsilon)]^{1/2})$. The appropriate scaling for $\tilde{\lambda}$ is then given by

$$\tilde{\lambda} = \frac{\Lambda}{[\ln(1/\epsilon)]^{1/2}}, \tag{3.5}$$

where $\Lambda = O(1)$. This scaling also corresponds to the lower limit in $\tilde{\lambda}$ for which (3.2) holds. Other choices of scaling for $\tilde{\lambda}$ are of course possible. Different scalings will describe different degrees of interactions between the dendrites. We have

chosen this scaling because it describes the interesting transition from isolated to array-modified tip dynamics.

Having chosen a scaling for $\tilde{\lambda}$ the scaling for $\tilde{a}$ then follows from the conservation of heat condition (2.19) and the definition of ϵ (3.3). We thus let

$$\tilde{a} = \epsilon A, \tag{3.6}$$

where $A = O(1)$. The conservation of heat condition (2.19) then becomes

$$\pi A^2 = \Lambda^2. \tag{3.7}$$

The appropriate scaling for describing the dendrite shape $\tilde{R}(z, \theta)$ is the same as that for the characteristic dendrite radius $\tilde{a}$, namely,

$$\tilde{R}(z, \theta) = \epsilon R(z, \theta). \tag{3.8}$$

It then follows from (2.18) that

$$\pi A^2 = \lim_{z \to -\infty} \int_0^{2\pi} \int_0^{R(z,\theta)} \bar{r}\, \mathrm{d}\bar{r}\, \mathrm{d}\theta, \tag{3.9}$$

where $\bar{r} = r/\epsilon$.

In addition to the characteristic lengths $\tilde{\rho}$, $\tilde{a}$ and $\tilde{\lambda}$ there is another length scale, $\tilde{l}_{\text{decay}}$, which describes the distance behind the tip over which the dendrites approach equilibrium. This "decay length" sets the scale for z variations in Θ and R. For the $\tilde{\lambda}$ scaling we have chosen $\tilde{l}_{\text{decay}} = O(1)$. If we had chosen $\tilde{\lambda} = O(1)$ then $\tilde{l}_{\text{decay}} = O[\ln(1/\epsilon)]$. For either of these scalings the decay length is large relative to the radius of the dendrite. This means that the dendrites are slender in shape – shape variations $\partial R/\partial z$ along the length of the dendrite are gradual except near the tip. Because the dendrites are slender we can take advantage of slender-body theory [14] to describe the gradually varying shape of the dendrite.

We now construct a formal perturbation solution to the free-boundary problem in terms of the small parameter ϵ using the scalings (3.3)–(3.9) for which $\tilde{\rho} \ll \tilde{a} \ll \tilde{\lambda} \ll \tilde{l}_{\text{decay}}$. Our approach is similar to that used by Xu [16] in the analysis of an isolated dendrite in the small undercooling limit. We focus our attention on the "center" dendrite at $x = y = 0$ and divide the domain into three regions (see Fig. 2). The "inner" region is the near-dendrite region behind the tip and is described by $r = O(\epsilon)$, and $|z| = O(1)$ with $z < 0$. The "outer" region is the interdendritic region where $r = O(\tilde{\lambda})$ and each dendrite appears as a line extending from $z = 0$ to $z = -\infty$. The "tip" region describes the small region in the vicinity of the dendrite tip where $r = O(\epsilon^2)$ and $z = O(\epsilon^2)$. In each of the three regions we solve the governing equations as an asymptotic series in the small undercooling. Then, by requiring the solutions to match in the appropriate overlap regions we determine a uniformly valid solution for the whole domain.

3.1. Inner solution

The inner region is the near-dendrite region away from the tip. We use cylindrical coordinates where $\bar{r} = r/\epsilon$ and $|z| = O(1)$ with $z < 0$ to describe the inner temperature field $\Theta^{\text{in}}(\bar{r}, z, \theta)$. The governing equations for Θ^{in} are

$$\frac{1}{\bar{r}} \frac{\partial}{\partial \bar{r}} \left(\bar{r} \frac{\partial \Theta^{\text{in}}}{\partial \bar{r}} \right) + \frac{1}{\bar{r}^2} \frac{\partial^2 \Theta^{\text{in}}}{\partial \theta^2} + \epsilon^2 \left(\frac{\partial^2 \Theta^{\text{in}}}{\partial z^2} + \frac{\partial \Theta^{\text{in}}}{\partial z} \right) = 0 \quad \text{in } \bar{r} > R(z, \theta), \tag{3.10}$$

with the boundary conditions

$$\Theta^{\text{in}} = 1 \quad \text{on } \bar{r} = R(z, \theta), \tag{3.11}$$

$$\frac{1}{\ln(1/\epsilon)} \frac{\partial R}{\partial z} = \frac{\partial \Theta^{\text{in}}}{\partial \bar{r}} - \frac{1}{R^2} \frac{\partial R}{\partial \theta} \frac{\partial \Theta^{\text{in}}}{\partial \theta} - \epsilon^2 \frac{\partial R}{\partial z} \frac{\partial \Theta^{\text{in}}}{\partial z} \quad \text{on } \bar{r} = R(z, \theta), \tag{3.12}$$

and

$$\Theta^{\text{in}} \to 1 \quad \text{as } z \to -\infty. \tag{3.13}$$

In the inner region the only effect of the neighboring dendrites is to modify the far-field temperature which must be matched as $\bar{r} \to \infty$. The equations suggest an expansion in powers of ϵ^2 and $\delta = 1/\ln(1/\epsilon)$. We expect that at leading order the temperature field and the dendrite shape are axisymmetric. In fact it turns out (see Appendix C) that asymmetry does not appear until $O(\epsilon^4)$. We thus expand Θ^{in} and R as

$$\Theta^{\text{in}}(\bar{r}, z, \theta) = \Theta_0^{\text{in}}(\bar{r}, z) + \delta \Theta_1^{\text{in}}(\bar{r}, z) + O(\delta^2) \tag{3.14}$$

and

$$R(z, \theta) = R_0(z) + \delta R_1(z) + O(\delta^2). \quad (3.15)$$

Formally the expansions (3.14) and (3.15) contain terms which have powers of ϵ^2, however, since $\delta^N \gg \epsilon^2$ for all $N > 1$, the ϵ^2 terms do not appear until infinite order in δ. Upon substitution of the expansions into the governing equations we find the first two terms in the expansion for the temperature field to be

$$\Theta_0^{\text{in}}(\bar{r}, z) = 1 \quad (3.16)$$

and

$$\Theta_1^{\text{in}}(\bar{r}, z) = B_1(z) \ln\left(\frac{\bar{r}}{R_0(z)}\right). \quad (3.17)$$

In the above equation $R_0(z)$ satisfies the differential equation

$$\frac{dR_0}{dz} = \frac{B_1(z)}{R_0(z)} \quad (3.18)$$

subject to the boundary condition $R_0(0) = 0$. The unknown function $B_1(z)$ must satisfy

$$B_1(z) \to 0 \quad \text{as } z \to -\infty \quad (3.19)$$

and is determined by matching the inner solution to the outer solution.

3.2. Outer solution

In the outer region x and y are on the scale of the dendrite spacing $\tilde{\lambda}$. Since $\tilde{a} \ll \tilde{\lambda}$, each dendrite looks like a line source of heat extending from $z = 0$ to $z = -\infty$. The temperature field in the outer region can thus be represented as a sum over an array of half-line sources,

$$\Theta^{\text{out}}(x, y, z) = \sum_{i=-\infty}^{\infty} \sum_{j=-\infty}^{\infty} \int_{-\infty}^{0} \tilde{q}(z') \times G\left(x, y, z; i\tilde{\lambda}, j\tilde{\lambda}, z'\right) dz', \quad (3.20)$$

where $\tilde{q}(z')$ is the strength of a half-line heat source with $\tilde{q}(z') = 0$ for $z' > 0$, and where $G(x, y, z; x', y', z')$ is the free-space Green's function given by

$$G(x, y, z; x', y', z') = \frac{1}{4\pi} \frac{\exp\{-\frac{1}{2}[|x - x'| + (z - z')]\}}{|x - x'|}, \quad (3.21)$$

where x is the vector $x = (x, y, z)$. The solution for Θ^{out} given by (3.20) is a formal solution to the diffusion equation (2.10) which satisfies the far field condition (2.14). It also satisfies the equilibrium condition (2.15) provided the total heat released by a single line source is equal to the latent heat released by a single dendrite,

$$\int_{-\infty}^{0} \tilde{q}(z')\, dz' = \frac{\pi \tilde{a}^2}{\sigma} = \tilde{\lambda}^2 = \frac{\Lambda^2}{\ln(1/\epsilon)}. \quad (3.22)$$

From this heat balance the appropriate scaling for $\tilde{q}(z')$ is

$$\tilde{q}(z') = \delta q(z'), \quad (3.23)$$

which agrees with our earlier scaling arguments. The conservation condition for $q(z')$ follows from (3.22) and is given by

$$\int_{-\infty}^{0} q(z')\, dz' = \Lambda^2. \quad (3.24)$$

The functional form for the source strength $q(z')$ is determined by matching with the inner solution.

To the order that the inner solution has been determined, all we require for matching is the line source $q(z')$ subject to (3.24). Matching at higher orders will require an expansion for $q(z')$ in powers of δ and ϵ^2. In addition, it will also be necessary to introduce higher-order line-source singularities (like quadrupoles) to account for the nonaxisymmetric features of the temperature field. As will be shown in Appendix C, these nonaxisymmetric effects do not appear until at least $O(\epsilon^4)$ because this is the order at which the dendrite feels the pattern of the array.

3.3. Tip solution

In the vicinity of the tip the appropriate scalings are $(x, y, z, r) = \epsilon^2(x_+, y_+, z_+, r_+)$ with the surface described by $r_+ = R_+(z_+, \theta) =$

$\epsilon^2 R(z, \theta)$. The governing equations for the temperature in the tip region $\Theta^{\text{tip}}(x_+, y_+, z_+)$ are

$$\frac{\partial^2 \Theta^{\text{tip}}}{\partial x_+^2} + \frac{\partial^2 \Theta^{\text{tip}}}{\partial y_+^2} + \frac{\partial^2 \Theta^{\text{tip}}}{\partial z_+^2} + \epsilon^2 \frac{\partial \Theta^{\text{tip}}}{\partial z_+} = 0$$

in the liquid, (3.25)

with the boundary conditions

$$\Theta^{\text{tip}} = 1 \quad \text{on } r_+ = R_+(z_+, \theta), \tag{3.26}$$

and

$$\frac{n_z}{\ln(1/\epsilon)} + \boldsymbol{n} \cdot \nabla \Theta^{\text{tip}} = 0 \quad \text{on } r_+ = R_+(z_+, \theta). \tag{3.27}$$

The far field conditions on Θ^{tip} are that it match with the inner and outer solutions.

We solve for Θ^{tip} and R_+ as expansions in $\delta = 1/\ln(1/\epsilon)$ and ϵ^2. As with the inner solution we can assume the leading order terms are axisymmetric,

$$\Theta^{\text{tip}}(r_+, z_+, \theta) = \Theta_0^{\text{tip}}(r_+, z_+) + \delta \Theta_1^{\text{tip}}(r_+, z_+) + O(\delta^2) \tag{3.28}$$

and

$$R_+(z_+, \theta) = R_0^+(z_+) + \delta R_1^+(z_+) + O(\delta^2). \tag{3.29}$$

Eqs. (3.25)–(3.27) governing the tip region are identical to those describing solidification of an isolated dendrite in the small Peclet number limit except no far-field condition is prescribed. The equations admit an axisymmetric similarity solution which corresponds to the Ivantsov solution in the limit of small undercooling,

$$\Theta^{\text{tip}} = 1 - \delta \eta_0 \ln(\eta/\eta_0) + O(\delta^2), \tag{3.30}$$

where the similarity variable is given by

$$\eta = \tfrac{1}{2}\left[\sqrt{r_+^2 + z_+^2} + z_+\right]. \tag{3.31}$$

The solid boundary is given by $\eta = \eta_B$ (constant) with

$$\eta_B = \eta_0 + \delta \eta_1 + O(\delta^2). \tag{3.32}$$

The surface is thus given by

$$R_+(z_+) = 2\sqrt{\eta_0(\eta_0 - z_+)} + O(\delta), \tag{3.33}$$

where η_0 is related to the scaled Peclet number of the dendrite tip by

$$\eta_0 = P/2. \tag{3.34}$$

The constant P is an unknown. In the isolated dendrite problem it is determined by the far-field conditions. Here it is determined by matching the tip solution to both the inner and outer solutions.

3.4. Matching of solutions

The details of matching the inner and outer solutions are given in Appendix A. Matching requires that the line source strength of the outer solution satisfy the integral equation (A.14). The solution to this integral equation is

$$q(z) = \mu \Lambda^2 \, e^{\mu z}, \tag{3.35}$$

where

$$\mu = -1/2 + \sqrt{1/4 + 2\pi/\Lambda^2}. \tag{3.36}$$

The resulting inner solution is

$$\Theta^{\text{in}}(\bar{x}, \bar{y}, z) = 1 + \delta \frac{\mu \Lambda^2}{2\pi} e^{\mu z} \ln\left(\frac{\bar{r}}{R_0(z)}\right) + O(\delta^2), \tag{3.37}$$

with the leading-order shape of the dendrite given by

$$R_0(z) = \frac{\Lambda}{\sqrt{\pi}} \sqrt{1 - e^{\mu z}}. \tag{3.38}$$

Matching the tip solution to the inner and outer solutions (see Appendix B) determines the scaled Peclet number in terms of the array spacing,

$$P = \frac{\mu \Lambda^2}{2\pi} = \frac{1}{1 + \mu}. \tag{3.39}$$

4. Results

To leading order the dendrite shape is given by (3.38) and (3.36) with the scaled Peclet number P given by (3.39). These results describe a family of solutions which depend on the dendrite spacing parameter Λ. Fig. 3 shows the variation of the

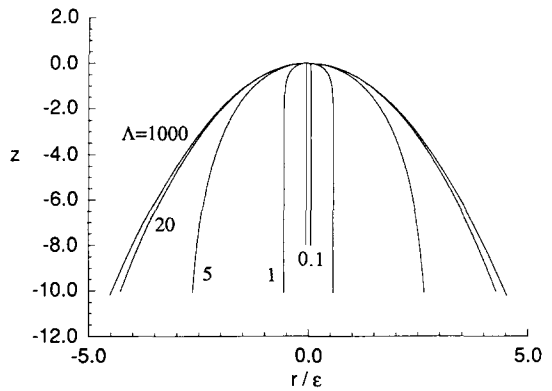

Fig. 3. Steady-state dendrite shapes $r/\epsilon = R_0(z)$ for different dendrite spacings Λ. The Ivantsov dendrite is recovered as $\Lambda \to \infty$.

shape of the needle crystal for different values of Λ.

In the large spacing limit, $\Lambda \to \infty$, $P \to 1$, and we recover the isolated dendrite. The tips behave as if they were isolated, growing into an undercooling of $\Delta\Theta = 1$. The dendrite shape deviates from the Ivantsov shape only when $|z| = O(\Lambda^2) \gg 1$. The radius of the dendrite then tends to a constant value $\Lambda/\pi^{1/2}$ as $|z|/\Lambda^2 \to \infty$.

For intermediate spacings, $\Lambda = O(1)$ and $0 < P < 1$. The dendrite tip is paraboloidal but the Peclet number is smaller than that for an isolated dendrite. The Peclet number is smaller because the dendrite tips feel the effect of the array as a reduced undercooling. In the absence of the array the tip would be growing into a far field with $\Theta = 0$ and unit undercooling $\Delta\Theta = 1$. When the array is present it generates a temperature increase in the vicinity of the tip given by $\Theta^{\text{array}}(0, 0, 0) = \mu/(1+\mu)$. Thus the tip sees a *modified undercooling* given by

$$\Delta\Theta = 1 - \frac{\mu}{1+\mu} = \frac{1}{1+\mu}. \tag{4.1}$$

The Peclet number reflects this modified undercooling. Recall that the Ivantsov solution satisfies (3.1). In our scalings the effective undercooling which the tip feels is $\sigma = \Delta\Theta\epsilon^2 \ln(1/\epsilon)$ with $\tilde{\rho} = \epsilon^2 P$. The Ivantsov relation (3.1) becomes $\Delta\Theta \sim P$ which is precisely that found in Eqs. (3.39) and (4.1). The dendrite tip, then, is paraboloidal with a Peclet number given by a modified undercooling due to the presence of the array. Deviations from this paraboloidal shape occur for $|z| = O(1)$ with the dendrite radius approaching a constant value as $z \to -\infty$.

In the small spacing limit, $\Lambda \to 0$, and the modified undercooling approaches zero because of strong interactions between dendrites. Thus the scaled Peclet number also approaches zero. On the scale of the diffusion length l the dendrites appear to be vanishingly thin cylinders of constant radius with a boundary-layer cap of thickness $|z| = O(\Lambda) \ll 1$ in which the transition from tip to equilibrium takes place.

The one-parameter family of solutions for the dendritic array has one more degree of freedom than the isolated dendrite. For the isolated dendrite there is no unique velocity prescribed, only the ratio $\rho/l \propto \rho V$ is determined, leaving one degree of freedom. Here the array has two degrees of freedom which can be thought of as the spacing and the tip radius. Specifying both of these prescribes a unique velocity.

We can isolate the velocity dependence in our array solutions by introducing a length scale, say the capillary length d_0, which is independent of V. Then by defining a dimensionless velocity, tip radius, and dendrite spacing as

$$V' = \frac{1}{\epsilon^4}\frac{d_0}{l}, \tag{4.2}$$

$$\rho' = \epsilon^2 \frac{\rho}{d_0}, \tag{4.3}$$

and

$$\lambda' = \epsilon^4 [\ln(1/\epsilon)]^{1/2} \frac{\lambda}{d_0}, \tag{4.4}$$

respectively, we obtain

$$\Lambda = \lambda' V' \tag{4.5}$$

and

$$P = \rho' V'. \tag{4.6}$$

Using (3.36) and (3.39), we solve for the velocity as a function of tip radius ρ' and dendrite spacing λ' to find

$$V' = \frac{1}{\rho'}\left[1 - 2\pi\left(\frac{\rho'}{\lambda'}\right)^2\right]. \tag{4.7}$$

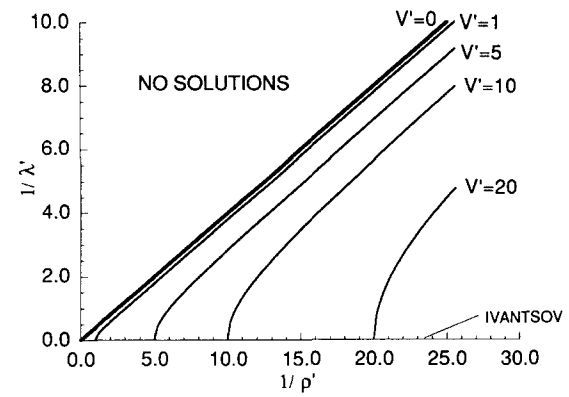

Fig. 4. Steady-state array velocity V' as a function of the tip radius ρ' and the dendrite spacing λ'. Contours correspond to surfaces of constant velocity. No steady-state solutions exist above the line $V' = 0$. The lower axis $1/\lambda' = 0$ corresponds to the Ivantsov dendrite.

Relation (4.7) is an important result of our work. It describes the compatible choices of V', ρ' and λ' for steady-state growth in the limit of small undercooling. The surface described by (4.7) is shown in Fig. 4. Any state selected by the array must lie on this surface in the same way that the state selected by a free dendrite is described by an Ivantsov solution. For a given velocity, the effect of a finite spacing is to decrease the tip radius from its isolated-dendrite value. The intersection of the solution surface with $V' = 0$ gives the nonphysical limit of an infinite diffusion length l which corresponds to $\Lambda = 0$ in our parameters. This intersection gives the boundary for physically admissible choices of λ' and ρ'.

The two degrees of freedom present in our steady-state solutions are consistent with studies of solidification in insulated channels [8,10]. Including the effect of surface energy removes one of the degrees of freedom. In particular, numerical calculations for the one-sided model [17,18] indicate that if the surface energy is isotropic then there are no solutions. If the surface energy is anisotropic then there is a unique velocity for a given spacing. We expect that a similar selection criterion will apply to our solutions. The other degree of freedom corresponds to the dendrite spacing. The selection of a dendrite spacing in the context of our model would be accomplished by a stability analysis of the array using methods similar to those of Warren and Langer [11] in the study of dendritic arrays in directionally solidified two-component melts. In their case it was found that a range of spacings are stable for a given growth velocity. In directional solidification, however, there is an imposed vertical temperature gradient which acts to inhibit dendritic growth and is responsible for the existence of the range of stable spacings. In our case there is no such stabilizing influence and we expect that all array spacings are unstable. Physically, the instability would manifest itself as a "coarsening" of the array. This tendency is reflected in Eq. (4.7) and Fig. 4. For any fixed tip radius (presumably determined by a tip selection criterion) the velocity of the dendrites always increases as λ increases. The growth of perturbations which increase the spacing of the array are thus favored by a faster growth rate for the array; any perturbation to the array which causes the tip of one dendrite to advance ahead of the rest would result in the dendrite growing out ahead of the array. Thus, in the long-time limit we expect the system to tend to arrays with very large spacings.

Our results for the steady-state dendritic array can also be interpreted in terms of a macroscopic description of the average temperature field. This average temperature field is a cross-sectional average over x and y as a function of z. The dominant contribution to this average is due to the "outer" field. The "inner" field appears only as a small correction to the macroscopic description since the volume fraction occupied by the dendrites is proportional to the small undercooling. To leading order, the average temperature profile is

$$\Theta = \begin{cases} \mu\, \mathrm{e}^{-z}/(\mu+1) & \text{for } z > 0, \\ 1 - \mathrm{e}^{\mu z}/(\mu+1) & \text{for } z < 0, \end{cases} \tag{4.8}$$

where the interaction parameter μ is given in terms of physical lengths and the undercooling as

$$\mu = 2\pi\rho l/\sigma\lambda^2. \tag{4.9}$$

This representation for the interaction parameter allows for an estimation of the dendritic interac-

tions as $\sigma \to 0$ when $\lambda \ll l$. These results could also be used in a mushy-layer model for dendritic growth. They provide a temperature boundary condition for the mush/liquid interface as well as a "decay length" for the temperature field in the mushy layer which are linked to the dendrite spacing through the parameter μ.

Our results are also directly applicable to crystal growth from a two-component supersaturated solution at a fixed temperature. In the one-sided model for alloy solidification (see Refs. [8,19]) the release of latent heat is negligible; growth is controlled by the diffusion of solute in the liquid with no diffusion in the solid. If C is the concentration field of the liquid, C_0 is the equilibrium liquid concentration, ΔC is the far-field supersaturation, D is the solute diffusivity, and k is the segregation coefficient, then the nondimensional equations describing steady-state growth are equivalent to (2.10)–(2.15) where $l = D/V$, $\Theta = (C - C_0 - \Delta C)/\Delta C$ and $\sigma = \Delta C/C_0(1-k)$. These substitutions convert our results to describe isothermal crystal growth from a two-component supersaturated solution.

Finally, an important aspect of our results is that to leading order they are independent of the pattern chosen for the array. This is because the dominant contribution to Θ^{array} is from the $k = l = 0$ term in the eigenfunction expansion for $\mathcal{G}$ (see Appendix C). This term is the same for any pattern, and depends only on the area of the pattern $\tilde{\lambda}^2$. Thus our leading-order results, which are derived explicitly for square arrays, are also valid for hexagonal and rectangular arrays. Furthermore, since our regular array is really nothing more than a three-dimensional channel with no-flux boundary conditions, our results are also applicable to three-dimensional channels with various cross-sectional geometries. Among these are circular, square, rectangular and hexagonal cylinders. Our results can thus be applied to channel growth experiments when $\sigma \to 0$, $\lambda/l \to 0$. While this in principle poses no difficulty, the appearance of $1/\ln(1/\epsilon)$ in our scaling for λ/l imposes a practical constraint on how small the undercooling needs to be. In particular, for our analysis of strong interactions to be relevant in an experiment, the undercooling must be small enough that $1/\ln(1/\epsilon) \ll 1$. A conservative choice of $1/\ln(1/\epsilon) = 0.1$ requires an extremely small undercooling of $\sigma = 2 \times 10^{-8}$. Even a more generous choice of $1/\ln(1/\epsilon) = 0.2$ requires $\sigma = 2 \times 10^{-4}$. To our knowledge, no channel growth experiments have yet been conducted at small enough undercoolings to test the predictions of our theory and its range of validity.

5. Conclusions

We have considered the steady-state growth of a pure material into an undercooled melt as an array of identical three-dimensional dendrites in the absence of surface energy. We have determined analytical solutions to the steady-state free-boundary problem as an expansion in the small undercooling using slender-body theory where each dendrite in the array appears as a line source of heat which decays exponentially behind the tip. In the limit of small undercooling, dendrite interactions are only important at the tip if the dendrite spacing is much less than the diffusion length. In this case the Peclet number of the dendrite tip is determined by the *modified undercooling* due to the presence of the array instead of the far-field undercooling. The steady-state solutions have two degrees of freedom which we use to determine explicitly the dendrite velocity as a function of the tip radius and the dendrite spacing. In the limit of large spacings we recover the dynamics of the Ivantsov dendrite. Our leading-order results for the array are valid for any space-filling array pattern as well as for solidification in insulated channels of various shapes. From our solutions we can describe the macroscopic behavior of the temperature field associated with the array in terms of the interaction parameter μ. These results include the interface temperature of the solidification front and the decay length of the temperature field behind the tips. The results presented here for solidification of a pure melt can also be directly converted to describe the isothermal solidification of a two-component supersaturated solution by making use of the one-sided model.

Acknowledgements

We would like to thank D.M. Anderson, S.H. Davis, R.C. Kerr, J.R. Lister and M.G. Worster for their critical reading of the manuscript and many beneficial discussions. This research is funded by a grant from the SERC.

Appendix A: Matching inner and outer solutions

The outer and inner solutions are matched in an intermediate region defined by

$$(x_*, y_*, r_*) = \frac{1}{\epsilon^\alpha}(x, y, r) = \epsilon^{1-\alpha}(\bar{x}, \bar{y}, \bar{r}) \quad \text{for } 0 < \alpha < 1, \tag{A.1}$$

where $z < 0$, and x_*, y_*, r_* and $|z|$ are O(1). The expansion for Θ^{in} in the intermediate region is straightforward,

$$\Theta^{\text{in}} = 1 + (1-\alpha)B_1(z) + \mathrm{O}(\delta). \tag{A.2}$$

The expansion for Θ^{out} in the intermediate region is more difficult. The derivation is somewhat lengthy because it is necessary to find an alternative representation for the double infinite series in (3.20).

We first note that for $(x, y) = \epsilon^\alpha(x_*, y_*) \to 0$ the largest contribution to the sum in (3.20) is due to the "center" source $i = j = 0$ when $x' = y' = 0$. The rest of the line sources ($i^2 + j^2 \neq 0$) are all much farther away from the near-inner intermediate region we are interested in and make significantly smaller contributions. We thus separate the sum in (3.20) into two pieces,

$$\Theta^{\text{out}} = \Theta^{\text{near}} + \Theta^{\text{array}}, \tag{A.3}$$

where Θ^{near} is the contribution of the nearest line source and Θ^{array} is the contribution of the rest of the line sources in the array. These terms are given explicitly by

$$\Theta^{\text{near}}(x, y, z) = \delta\int_{-\infty}^{0} \frac{q(z')}{4\pi} \frac{\exp\left\{-\frac{1}{2}\left[\sqrt{r^2 + (z-z')^2} + (z-z')\right]\right\}}{\sqrt{r^2 + (z-z')^2}}\, \mathrm{d}z' \tag{A.4}$$

and

$$\Theta^{\text{array}}(x, y, z) = \delta \sum_{\substack{i=-\infty \\ i^2+j^2\neq 0}}^{\infty} \sum_{j=-\infty}^{\infty} \int_{-\infty}^{0} q(z') G\left(x, y, z; i\tilde{\lambda}, j\tilde{\lambda}, z'\right) \mathrm{d}z'. \tag{A.5}$$

For $r = \epsilon^\alpha r_*$, $z < 0$, the integral in (A.4) is dominated by the contribution from the near-singularity at $z = z'$ which generates a factor of $\ln(1/\epsilon^\alpha)$. This behavior can be extracted by adding and subtracting a factor involving $q(z)$,

$$\Theta^{\text{near}}(x, y, z) = \delta\frac{q(z)}{4\pi}\int_{-\infty}^{0} \frac{\exp\left\{-\frac{1}{2}\left[\sqrt{r^2 + (z-z')^2} + (z-z')\right]\right\}}{\sqrt{r^2 + (z-z')^2}}\, \mathrm{d}z'$$

$$+ \delta\int_{-\infty}^{0} \frac{[q(z') - q(z)]}{4\pi} \frac{\exp\left\{-\frac{1}{2}\left[\sqrt{r^2 + (z-z')^2} + (z-z')\right]\right\}}{\sqrt{r^2 + (z-z')^2}}\, \mathrm{d}z'. \tag{A.6}$$

The first term can be integrated explicitly by making the change of variable

$$\zeta(z') = \tfrac{1}{2}\left[\sqrt{r^2 + (z-z')^2} + (z-z')\right], \tag{A.7}$$

to find

$$\Theta^{\text{near}}(x, y, z) = \delta\frac{q(z)}{4\pi}E_1[\zeta(0)] + \delta\int_{-\infty}^{0}\frac{[q(z')-q(z)]}{4\pi}\frac{\exp\left\{-\tfrac{1}{2}\left[\sqrt{r^2+(z-z')^2}+(z-z')\right]\right\}}{\sqrt{r^2+(z-z')^2}}\,dz', \tag{A.8}$$

where $E_1(\zeta)$ is the exponential integral. The asymptotics of (A.8) for $r = \epsilon^{\alpha}r_*$, $z < 0$ are straightforward. The $E_1[\zeta(0)]$ gives a factor of $\ln(1/\epsilon^{\alpha})$. The integral in the second term is well behaved and O(1). Thus

$$\Theta^{\text{near}}(\epsilon^{\alpha}x_*, \epsilon^{\alpha}y_*, z) = \frac{\alpha q(z)}{2\pi} + O(\delta). \tag{A.9}$$

Now consider Θ^{array} as given by (A.5). For $(x, y) = \epsilon^{\alpha}(x_*, y_*)$, $z < 0$, the Green's function can be formally expanded in powers of $\epsilon^{\alpha}/\tilde{\lambda}$. The leading term of this expansion is

$$\Theta^{\text{array}}(\epsilon^{\alpha}x_*, \epsilon^{\alpha}y_*, z) \sim \delta\sum_{\substack{i=-\infty \\ i^2+j^2\neq 0}}^{\infty}\sum_{j=-\infty}^{\infty}\int_{-\infty}^{0} q(z')G(0, 0, z; i\tilde{\lambda}, j\tilde{\lambda}, z')\,dz', \tag{A.10}$$

which is independent of x_* and y_*. The difficulty with this approach is that this sum converges very slowly in i, j because $\tilde{\lambda} = O(\delta^{1/2}) \ll 1$. We need an alternative representation for Θ^{array} which makes advantageous use of $\tilde{\lambda} \ll 1$.

The alternative representation can be found by replacing the sum of sources in (A.5) by an equivalent heat flux on the walls of the center cell. The details of this calculation are given in Appendix C. The result is

$$\Theta^{\text{array}}(\epsilon^{\alpha}x_*, \epsilon^{\alpha}y_*, z) = \frac{1}{\Lambda^2}\left(\int_z^0 q(z_0)\,dz_0 + \int_{-\infty}^{z} q(z_0)\exp(z_0 - z)\,dz_0\right) + O(\delta). \tag{A.11}$$

A consequence of (A.11) is that to leading order Θ^{array} is independent of x_* and y_*, varying only in z. As indicated in Appendix C, the symmetry of Θ^{array} means that the inner temperature field is axisymmetric until $O(\epsilon^4\delta^3)$.

We can now complete the matching of Θ^{in} and Θ^{out} in the overlap region. We have Θ^{in} given by (A.2) and

$$\Theta^{\text{out}} = \frac{\alpha q(z)}{2\pi} + \frac{1}{\Lambda^2}\left(\int_z^0 q(z_0)\,dz_0 + \int_{-\infty}^{z} q(z_0)\exp(z_0 - z)\,dz_0\right) + O(\delta). \tag{A.12}$$

Matching determines

$$B_1(z) = -q(z)/2\pi, \tag{A.13}$$

with $q(z)$ determined by the integral equation

$$\frac{q(z)}{2\pi} + \frac{1}{\Lambda^2}\left(\int_z^0 q(z_0)\,dz_0 + \int_{-\infty}^{z} q(z_0)\exp(z_0 - z)\,dz_0\right) = 1. \tag{A.14}$$

The solution to the integral equation can be found by differentiating Eq. (A.14) with respect to z, substituting for the integral that remains using (A.14), and differentiating again to obtain a homogeneous second-order ordinary differential equation with constant coefficients. The two solutions to the differential equation are exponentials. One of the exponentials becomes infinite as $z \to -\infty$ and is discarded. The other has the proper decay as $z \to -\infty$. The arbitrary coefficient multiplying the solution to the homogeneous differential equation is determined by substitution of the exponential solution into the integral equation (A.14). The resulting solution is

$$q(z) = \mu \Lambda^2 \, e^{\mu z}, \tag{A.15}$$

where

$$\mu = -1/2 + \sqrt{1/4 + 2\pi/\Lambda^2}\,. \tag{A.16}$$

Solution (A.15) satisfies the conservation of heat constraint (3.24) automatically. Having determined $q(z)$ and $B_1(z)$ from matching, we can now solve explicitly for the shape $R_0(z)$ from (3.18). The result is

$$R_0(z) = \frac{\Lambda}{\sqrt{\pi}} \sqrt{1 - e^{\mu z}}\,. \tag{A.17}$$

The accompanying inner temperature field is given in final form as

$$\Theta^{\text{in}}(\bar{x}, \bar{y}, z) = 1 + \delta \frac{\mu \Lambda^2}{2\pi} \, e^{\mu z} \ln\left(\frac{\bar{r}}{R_0(z)}\right) + O(\delta^2). \tag{A.18}$$

This solution is valid everywhere near the surface of the dendrite except near the tip where $R_0 \to 0$ and $dR_0/dz \gg 1$. The details of the tip region must be solved for separately and matched to the inner and outer solutions.

Appendix B: Matching the tip to inner and outer solutions

We first match the tip solution to the inner solution in the intermediate region where

$$r = \epsilon^{1+\alpha} r_\dagger \quad \text{for } 0 < \alpha < 1, \tag{B.1}$$

$$z = \epsilon^{2\beta} z_\dagger \quad \text{for } z_\dagger < 0 \text{ and } 0 < \beta < 1, \tag{B.2}$$

and

$$R(z, \theta) = \epsilon^{1+\alpha} R_\dagger(z_\dagger, \theta). \tag{B.3}$$

We restrict $2\beta < 1 + \alpha$ so that $r \ll |z|$ in the intermediate region but otherwise leave α and β as arbitrary.

Expanding the inner solution for $\bar{r} = \epsilon^\alpha r_\dagger$, $z = \epsilon^{2\beta} z_\dagger < 0$ and $R = \epsilon^\alpha R_\dagger$, we find that

$$\Theta^{\text{in}} = 1 - \frac{\mu \Lambda^2}{2\pi}(\beta - \alpha) + O(\delta) \tag{B.4}$$

and

$$R_\dagger^{\text{in}} = \sqrt{\frac{\mu \Lambda^2 |z_\dagger|}{\pi}} \, \epsilon^{\beta - \alpha} + O(\delta \epsilon^{\beta - \alpha}). \tag{B.5}$$

Expanding the tip solution for $r_+ = r_\dagger/\epsilon^{1-\alpha}$, $z_+ = z_\dagger/\epsilon^{2(1-\beta)}$ and $R_+ = R_\dagger/\epsilon^{1-\alpha}$, we obtain

$$\Theta^{\text{tip}} = 1 - 2\eta_0(\beta - \alpha) + O(\delta) \tag{B.6}$$

and

$$R_\dagger^{\text{tip}} = 2\sqrt{\eta_0 |\, z_\dagger|}\,\epsilon^{\beta-\alpha} + O(\delta\epsilon^{\beta-\alpha}). \tag{B.7}$$

Matching, we determine the constant η_0 as

$$\eta_0 = \mu\Lambda^2/4\pi. \tag{B.8}$$

Repeating the matching procedure in the intermediate region between the tip and the outer regions defined by $(x_\ddagger, y_\ddagger, z_\ddagger)$ where

$$(x, y, z) = \epsilon^{2\alpha}(x_\ddagger, y_\ddagger, z_\ddagger) \quad \text{for } 0 < \alpha < 1, \tag{B.9}$$

we obtain

$$\Theta^{\text{tip}} = 1 - 2\eta_0(1 - \alpha) + O(\delta) \tag{B.10}$$

and

$$\Theta^{\text{out}} = \frac{\alpha q(0)}{2\pi} + \frac{\mu}{\mu + 1} + O(\delta). \tag{B.11}$$

Matching is automatic with η_0 given by (B.8) and the three leading-order solutions now match in all the overlap regions.

Appendix C: Temperature field generated by the array

Here we determine the alternative representation for Θ^{array} given by (A.5). The alternative representation can be found by noting that Θ^{array} is a solution to the sourceless diffusion equation in the center cell $|x| < \tilde{\lambda}/2$, $|y| < \tilde{\lambda}/2$, with an effective heat flux on the cell walls corresponding to the effect of the dendrites in the array. This effective heat flux can be calculated explicitly by observing that $\sum_{i=-\infty}^{\infty}\sum_{j=-\infty}^{\infty} G(x, y, z; i\tilde{\lambda}, j\tilde{\lambda}, z')$ is the Green's function for a point source at $(x', y', z') = (0, 0, z')$ in an insulated center cell. If there is a line source in every cell then there is no flux on the walls of the cell $x = \pm\tilde{\lambda}/2$, $y = \pm\tilde{\lambda}/2$. The heat flux on the cell walls which is generated by the array of line sources with the center source missing must then be exactly that needed to cancel the heat flux on the cell walls due to the center source acting by itself. The sum of the "outer" sources ($i^2 + j^2 \neq 0$) can thus be formally replaced by a heat flux on the cell boundary which is given by the negative of that generated by a line source at the center of the cell. After calculating the heat flux on the boundary we can then solve for the temperature field in the cell using the Green's function for the insulated cell, $\mathcal{G}$, where we use an eigenfunction expansion for $\mathcal{G}$ which converges rapidly when $\tilde{\lambda} \ll 1$.

Since Θ^{array} has the symmetries $x \leftrightarrow -x$, $y \leftrightarrow -y$ and $(x, y) \leftrightarrow (y, x)$, we only need to solve for Θ^{array} in one quarter of the center cell, $0 < x < \tilde{\lambda}/2$ and $0 < y < \tilde{\lambda}/2$, where

$$\nabla^2\Theta^{\text{array}} + \frac{\partial\Theta^{\text{array}}}{\partial z} = 0. \tag{C.1}$$

The boundary conditions for (C.1) are

$$\frac{\partial \Theta^{\text{array}}}{\partial n} = f(y, z) \quad \text{on } x = \tilde{\lambda}/2, \tag{C.2a}$$

$$\frac{\partial \Theta^{\text{array}}}{\partial n} = f(x, z) \quad \text{on } y = \tilde{\lambda}/2, \tag{C.2b}$$

$$\frac{\partial \Theta^{\text{array}}}{\partial n} = 0 \quad \text{on } x = 0 \text{ and } y = 0, \tag{C.2c}$$

$$\frac{\partial \Theta^{\text{array}}}{\partial z} \to 0 \quad \text{as } |z| \to \infty, \tag{C.2d}$$

$$\Theta^{\text{array}} \to 0 \quad \text{as } z \to \infty. \tag{C.2e}$$

In the above boundary conditions $\partial/\partial n$ denotes the gradient in the direction of the outward normal to the cell boundary. The function $f(x, z)$ is the heat flux on $y = \tilde{\lambda}/2$ due to a line sink at $x = y = 0$ given by

$$f(x, z) = -\left.\frac{\partial \Theta^{\text{near}}}{\partial y}\right|_{y=\tilde{\lambda}/2} = -\delta \left.\int_{-\infty}^{0} q(z') \frac{\partial G}{\partial y}(x, y, z; 0, 0, z')\, \mathrm{d}z'\right|_{y=\tilde{\lambda}/2}. \tag{C.3}$$

The solution to (C.1) and (C.2) is given in terms of a Green's function $\mathcal{G}$ as

$$\Theta^{\text{array}}(x, y, z) = \int_{-\infty}^{\infty} \mathrm{d}z_0 \left.\int_0^{\tilde{\lambda}/2} \mathrm{d}x_0 \left[\mathcal{G}(x, y, z; x_0, y_0, z_0) + \mathcal{G}(x, y, z; y_0, x_0, z_0)\right] f(x_0, z_0)\right|_{y_0=\tilde{\lambda}/2}, \tag{C.4}$$

where $\mathcal{G}(\boldsymbol{x}; \boldsymbol{x}_0)$ is the Green's function for an insulated box $0 < x < \tilde{\lambda}/2$, $0 < y < \tilde{\lambda}/2$ which satisfies

$$-\nabla^2 \mathcal{G} - \frac{\partial \mathcal{G}}{\partial z} = \delta(\boldsymbol{x} - \boldsymbol{x}_0), \tag{C.5}$$

with

$$\frac{\partial \mathcal{G}}{\partial n} = 0 \quad \text{on } x = 0,\ x = \tilde{\lambda}/2,\ y = 0, \text{ and } y = \tilde{\lambda}/2, \tag{C.6}$$

$$\frac{\partial \mathcal{G}}{\partial z} \to 0 \quad \text{as } |z - z_0| \to \infty, \tag{C.7}$$

and

$$\mathcal{G} \to 0 \quad \text{as } (z - z_0) \to \infty. \tag{C.8}$$

The eigenfunction expansion for $\mathcal{G}$ is

$$\mathcal{G}(\boldsymbol{x}; \boldsymbol{x}_0) = \sum_{k=-\infty}^{\infty} \sum_{l=-\infty}^{\infty} \frac{4 \cos(2\pi k x_0/\tilde{\lambda}) \cos(2\pi l y_0/\tilde{\lambda}) \cos(2\pi k x/\tilde{\lambda}) \cos(2\pi l y/\tilde{\lambda})}{\tilde{\lambda}^2 \sqrt{1 + (4\pi/\tilde{\lambda})^2 (k^2 + l^2)}} \times \exp\left\{\tfrac{1}{2}(z - z_0)\left[-1 \pm \sqrt{1 + (4\pi/\tilde{\lambda})^2 (k^2 + l^2)}\right]\right\}, \tag{C.9}$$

where $+,-$ is understood to apply for $z < z_0$, $z > z_0$, respectively. Thus, after some rearranging,

$$\Theta^{\text{array}}(x, y, z) = \delta \int_{-\infty}^{\infty} \mathrm{d}z_0 \int_0^1 \mathrm{d}s\, \hat{\mathscr{G}}(\boldsymbol{x}, s, z_0) \int_{-\infty}^{0} \mathrm{d}z'\, q(z') \hat{G}(s, z_0, z'), \tag{C.10}$$

where

$$\hat{G}(s, z_0, z') = \frac{1}{4\pi} \exp\{-\tfrac{1}{2}[d + (z_0 - z')]\} \left(\frac{1}{2d^2} + \frac{1}{d^3} \right), \tag{C.11}$$

and

$$\hat{\mathscr{G}}(\boldsymbol{x}, s, z_0) = \sum_{k=-\infty}^{\infty} \sum_{l=-\infty}^{\infty} \frac{(-1)^l \cos(\pi k s)}{\sqrt{1 + (4\pi/\tilde{\lambda})^2 (k^2 + l^2)}} \psi_{kl}(x, y) \times \exp\left\{ \tfrac{1}{2}(z - z_0) \left[-1 \pm \sqrt{1 + (4\pi/\tilde{\lambda})^2 (k^2 + l^2)} \right] \right\}. \tag{C.12}$$

In the above expressions

$$d = \sqrt{(\tilde{\lambda}/2)^2 (1 + s^2) + (z_0 - z')^2} \tag{C.13}$$

and $\psi_{kl}(x, y)$ is the symmetric sum of the eigenfunctions given by

$$\psi_{kl}(x, y) = \cos(2\pi k x/\tilde{\lambda}) \cos(2\pi l y/\tilde{\lambda}) + \cos(2\pi l x/\tilde{\lambda}) \cos(2\pi k y/\tilde{\lambda}). \tag{C.14}$$

The integral representation (C.10) is an exact representation for the sum in (A.5). It contains an infinite sum as part of $\hat{\mathscr{G}}$, but this sum converges rapidly because $\tilde{\lambda} \ll 1$. In fact, the $k = l = 0$ term of the sum turns out to be asymptotically larger than the sum of the remaining terms, and the leading-order behavior of the integral requires only one term from the sum.

We are now in a position to determine the matching behavior of Θ^{array} for $(x, y) = \epsilon^{\alpha}(x_*, y_*)$, $z < 0$. To match with the inner solution we need the O(1) approximation to Θ^{array}. We let

$$\hat{\mathscr{G}} = \hat{\mathscr{G}}_0 + \hat{\mathscr{G}}_{\text{sum}}, \tag{C.15}$$

where $\hat{\mathscr{G}}_0$ is the $k = l = 0$ term of $\hat{\mathscr{G}}$, and $\hat{\mathscr{G}}_{\text{sum}}$ is the remaining terms for which $k^2 + l^2 \neq 0$. Since the z' integral is dominated by the contribution from $\hat{G}$ when $z' = z_0$ and $z' < 0$, we split the z_0 integral into two pieces,

$$\Theta^{\text{array}}(x, y, z) = \delta \int_{-\infty}^{0} \mathrm{d}z_0 \int_0^1 \mathrm{d}s \left[\hat{\mathscr{G}}_0(\boldsymbol{x}, s, z_0) + \hat{\mathscr{G}}_{\text{sum}}(\boldsymbol{x}, s, z_0) \right] \int_{-\infty}^{0} \mathrm{d}z'\, q(z') \hat{G}(s, z_0, z') + \delta \int_0^{\infty} \mathrm{d}z_0 \int_0^1 \mathrm{d}s \left[\hat{\mathscr{G}}_0(\boldsymbol{x}, s, z_0) + \hat{\mathscr{G}}_{\text{sum}}(\boldsymbol{x}, s, z_0) \right] \int_{-\infty}^{0} \mathrm{d}z'\, q(z') \hat{G}(s, z_0, z'). \tag{C.16}$$

In the second term all the functions are O(1) and well behaved, resulting in an overall $O(\delta)$ contribution. In the first term the dominant contribution to the z' integral occurs at the near-singularity in $\hat{G}$ at $z' = z_0$ which generates a factor of $\ln(1/\epsilon) = \delta^{-1}$. By the same approach used for determining (A.8) we find for $z_0 < 0$ that

$$\int_{-\infty}^{0} \mathrm{d}z'\, q(z') \hat{G}(s, z_0, z') = \frac{q(z_0)}{4\pi} \frac{\mathrm{e}^{-\zeta_0}}{\zeta_0^2 + (\tilde{\lambda}^2/16)(1 + s^2)} + \int_{-\infty}^{0} \mathrm{d}z'\, [q(z') - q(z_0)] \hat{G}(s, z_0, z'), \tag{C.17}$$

where

$$\zeta_0 = \tfrac{1}{2}\left[\sqrt{(\tilde{\lambda}^2/4)(1+s^2)+z_0^2}+z_0\right]. \tag{C.18}$$

Further, $\hat{\mathcal{G}}_0$ is O(1) while the terms in $\hat{\mathcal{G}}_{\text{sum}}$ are exponentially small except when $|z-z_0| = O(\tilde{\lambda})$, when the terms are $O(\tilde{\lambda})$ and decay rapidly in k, l. Thus the action of $\hat{\mathcal{G}}_0$ is O(1) and the action of $\hat{\mathcal{G}}_{\text{sum}}$ is $O(\delta)$. Expanding (C.17) for $\tilde{\lambda}^2 = \Lambda^2/\ln(1/\epsilon)$, substituting the result into (C.16) and integrating against $\hat{\mathcal{G}}_0$ as given by

$$\hat{\mathcal{G}}_0(\boldsymbol{x}, s, z_0) = \begin{cases} 2 & \text{for } z_0 > z, \\ 2\exp(z_0 - z) & \text{for } z_0 < z, \end{cases} \tag{C.19}$$

we obtain the desired leading-order result for Θ^{array},

$$\Theta^{\text{array}}(\epsilon^{\alpha}x_*, \epsilon^{\alpha}y_*, z) = \frac{1}{\Lambda^2}\left(\int_z^0 q(z_0)\,\mathrm{d}z_0 + \int_{-\infty}^{z} q(z_0)\exp(z_0 - z)\,\mathrm{d}z_0\right) + O(\delta). \tag{C.20}$$

Finally, Eq. (C.20) indicates that near the center dendrite the array generates a temperature field that to leading order is independent of x_* and y_*, varying only in z. The x_*, y_* dependence appears at $O(\delta)$ through the eigenfunctions $\psi_{kl}(x, y)$ in $\hat{\mathcal{G}}_{\text{sum}}$. An evaluation of these eigenfunctions in the matching region indicates that the appearance of nonaxisymmetry in Θ^{array} is of the form $\epsilon^{4\alpha}\delta^3 r_*^4 \times \sin(4\theta)$. Thus the inner temperature field does not require a nonaxisymmetric term until $O(\epsilon^4\delta^3)$.

References

[1] G.P. Ivantsov, Dokl. Akad. Nauk. SSSR 58 (1947) 567.
[2] S.C. Huang and M.E. Glicksman, Acta Metall. 29 (1981) 701.
[3] J.S. Langer and H. Müller-Krumbhaar, Acta Metall. 26 (1978) 1681.
[4] M. Ben Amar and E. Brener, Phys. Rev. Lett. 71 (1993) 589.
[5] E. Brener, Phys. Rev. Lett. 71 (1993) 3653.
[6] J.J. Xu and Z.X. Pan, J. Crystal Growth 129 (1993) 666.
[7] J.D. Verhoeven, Fundamentals of Physical Metallurgy (Wiley, New York, 1975) pp. 302–303.
[8] P. Pelce and A. Pumir, J. Crystal Growth 73 (1985) 337.
[9] P.G. Saffman and G.I. Taylor, Proc. Roy. Soc. London A 245 (1958) 312.
[10] J.D. Hunt, Acta Metall. Mater. 39 (1991) 2117.
[11] J.A. Warren and J.S. Langer, Phys. Rev. A 42 (1990) 3518.
[12] J.A. Warren and J.S. Langer, Phys. Rev. E 47 (1993) 2702.
[13] K. Somboonsuk, J.T. Mason and R. Trivedi, Metall. Trans. A 15A (1984) 967.
[14] E.J. Hinch, Perturbation Methods (Cambridge Univ. Press, Cambridge, 1992) pp. 87–90.
[15] D. Canright and S.H. Davis, Metall. Trans. A 20A (1989) 225.
[16] J.J. Xu, in: Structure and Dynamics of Partially Solidified Systems, Ed. D.E. Loper (Nijhoff, Dordrecht, 1987) p. 97.
[17] D.A. Kessler, J. Koplik and H. Levine, Phys. Rev. A 34 (1986) 4980.
[18] S.-Z. Lu and J.D. Hunt, J. Crystal Growth 123 (1992) 17.
[19] J.S. Langer, Rev. Mod. Phys. 52 (1980) 1.